MICROMECHANISTIC ANALYSIS OF TOUGHENED CARBON FIBRE COMPOSITE LAMINATE FAILURE BY HIGH RESOLUTION SYNCHROTRON COMPUTED TOMOGRAPHY

G. Borstnar[1]*, D. Bull[1], M.N.Mavrogordato[1], I. Sinclair[1], S.M. Spearing[1]
[1] Engineering Materials, University of Southampton, Southampton, United Kingdom
*(G.Borstnar@soton.ac.uk)

Keywords: *CFRP, Synchrotron Radiation Computed Tomography, Impact, Mode I, Mode II,*

Abstract
Synchrotron Radiation Computed Tomography (SRCT) allows for non-destructive identification of fracture mechanisms in materials at very high resolutions. In this work, carbon fibre reinforced plastics (CFRPs) were imaged using SRCT to ascertain fracture micro-mechanisms under both quasi-static Mode I and Mode II dominated loading conditions. This, combined with previous work on impacted coupons, provides mechanistic comparison between the different loading conditions on similar material systems. Initial findings have identified particle/matrix debonding, crack bridging and ligamented behaviour as reported previously, but have emphasized micro-cracks and the extent to which particle/matrix debonding occurs ahead of the crack tip under both Mode I and Mode II loading conditions. Such work is intended to support both material development and more accurate structural performance simulation for the toughened materials that are being increasingly used as primary structures in aerospace applications.

1 General Introduction

The use of composite materials on aircraft structures is increasing due to their desirable strength-to-weight and stiffness-to-weight properties. Whilst in service, composites may suffer from low velocity impact events, which have been shown to have a significant effect on the residual mechanical properties of the material [1]. As such, the need to resist impact damage, and the lack of reliable predictive models to account for damage, contribute to over-engineered structures and sub-optimal design [2].

The introduction of particles into polymer matrices has been developed as a toughening strategy for laminated composites over the past several decades. The effects of particle properties (modulus, size *etc.*) on the toughening mechanisms of composites has been subject to conventional post-mortem analyses, *e.g.* Groleau *et al.* who used destructive testing to identify the mechanisms occurring during Mode II fracture in an End Loaded Split (ELS) test using Transmission Optical Microscopy[3]. However, a wide variety of 3D imaging techniques can now be used to increase the understanding of these fracture mechanisms and hence build better models. The use of Computed Tomography (CT), in particular, allows for *in situ* observation and analysis of fracture mechanisms in a time-resolved, non-destructive manner, without introducing free surface artefacts [4].

In this work, Mode I and Mode II quasi-static fracture experiments are used to capture failure mechanisms under controlled loading conditions. Complementing previous low velocity impact data [5], the chronology of local damage evolution is assessed.

2 Methodology

2.1 Materials

CFRP test coupons for impact testing were manufactured using a 5mm thick quasi-isotropic 24 ply $[45\ 0\ -45\ 90]_{3S}$ lay-up. The pre-pregs were made of a proprietary intermediate modulus fibre (~7μm m diameter), and a ~30μm thick particle toughening interlayer.

Test coupons for Mode I and II fracture consisted of a 16 ply (3mm thick) uni-directional lay-up of the same intermediate modulus fibre, again with a ~30 μm thick particle toughened interleaf, containing chemically equivalent but smaller particles than the

impacted coupons: ~10μm versus ~30μm diameter respectively.

Mode I and Mode II specimen geometries compatible with CT imaging were employed: ideally, the specimens should be close to cylindrical, to provide uniform path lengths at all angles of rotation and to avoid artifacts. The specimens in this case were prepared with a 3x1mm cross-section and 120mm length, with a 10mm long, 40μm thick, PTFE starting defect (Fig. 1A). The small specimen size was required to allow sufficient transmission of low energy X-rays through the specimen and avoid image artefacts caused by material passing outside of the field of view.

2.2 Impact testing

The particle toughened systems were impacted according to ASTM D7136M standard, as reported in [5].

2.3 Mode I testing

In Mode I, a wedge-loaded double cantilever arrangement was used (Fig. 1B), which a metallic wedge (a scalpel blade) was driven into the resin rich region in the sample under displacement control. Guides kept the wedge vertical, with reasonably stable, self-similar growth being achieved. The samples were pre-cracked in Mode II before inserting the wedge as this was found to ensure the crack initiated within the resin rich region and not within the ply. Since the Mode I growth was extended for more than 1 cm before scanning, the effects of Mode II pre-cracking were assumed to be negligible.

2.4 Mode II testing

Mode II tests were performed using a similar 120mm x 3mm x 1mm wide specimen geometry, with a 10mm PTFE starter crack. These were pre-cracked a three-point bend configuration Crack growth was studied under an optical microscope prior to SRCT, to discern the approximate crack tip location.

2.5 Synchrotron Radiation Computed Tomography

SRCT was completed at the Swiss Light Source (SLS) on the TOMCAT beamline at the Paul Scherrer Institut, Villigen, Switzerland. A synchrotron generates an X-ray beam by accelerating electrons to almost the speed of light and putting them into an orbit. Bending magnets or insertion devices act on the electrons causing them to emitt X-rays that come off at a tangent of the synchroton to form a parallel beam used for SRCT. This varies from Micro-Focus CT that produces a cone beam by firing electrons at a metal target that then gives off X-rays.

The impacted samples were scanned at a voxel resolution of 1.4μm with a detector size of 2048x2048 pixels. The voxel resolution achieved for the Mode I and Mode II tests was 0.65μm, with a detector size of 2560 x 2160 pixels. A propagation distance of ~22mm was used, with near-field Fresnel diffraction fringes delineating the phase and crack edges over pure absorption imaging [6].

Reconstructions were conducted at the SLS via in-house GRIDREC method [7]. The subsequent volumes were analysed using ImageJ [8].

3 Results

3.1 Impact

Fig. 2 and Fig. 3 show typical cracking behaviour in a quasi-isotropic coupon. Fig. 2 shows a region ahead of the crack tip wherein several instances of isolated particle-resin de-bonding occur (highlighted at (i)). Fig. 3 identifies a ligamented fracture behaviour consisting of: (i) crack deflection around the particles, and (ii) particle bridging.

The micromechanical influence of the particles is clear from these images. The crack tip region is complex with no distinct crack front. In combination with the highly ligamented nature of failure, even once a contiguous crack is present, it is evident that traction may arise across the crack flanks, consistent with a cohesive zone approach to fracture modelling.

3.2 Mode II

Fig. 4 shows typical echelon behaviour (highlighted at (ii)) that has been previously identified in Mode II cracks [3]. Particle/matrix de-bonding, particle bridging, micro-cracking and crack coalescence to form a continuous crack are all micro-mechanisms that can be observed ahead of the crack tip in this image. These features are also present in the impacted sample. It is evident that the crack path follows particle-rich regions, as highlighted at (iii) in Fig. 4. Thicker resin rich regions have been reported to give increased echelon behaviour [9] and a more tortuous crack route [10], thus improving G_{IIC}. However, behaviour seen in Fig. 4 indicates that particle distribution and size also play a role in determining echelon crack morphology and hence may influence optimal interlayer thickness. This will require quantitative investigation, since thicker resin rich regions are formed at the cost of overall mechanical properties.

Fig. 5 highlights fracture micro-mechanisms ahead of the crack tip in relation to particle-depleted zones, showing small micro-cracks and echelon-like arrangements. Regions elsewhere in the reconstructed volumes show similar echelon crack behaviour, but with fewer deflections in crack path than in particle-rich regions, which tend to be much more tortuous. Fig. 5 shows several (i) particle-depleted zones, along with substantial (ii) particle/matrix de-bonding and coalescence far ahead of the crack tip. This suggests that particle/matrix de-bonding precedes (iii) cracking in the resin, *i.e.* toughening particles are preferential nucleation sites for crack growth via de-bonding [3]. Further 3D analysis showed that there was particle/matrix de-bonding on either side of undamaged particle-depleted zones (e.g. Fig. 5 (ii)), indicating that the cracks may grow around such zones initially, before cracking through them.

The local influence of a singular large particle in the resin rich layer is shown in Fig. 6, where a large de-bonding event has occurred. Fig. 7A shows the middle of the particle, and Fig. 7B a region ~30µm into surrounding material exhibiting a fine particle distribution. It is evident that scale and spatial density of initial damage events scales with the local particle population [3].

3.3 Mode I

The observation that macro-scale Mode II crack growth involves micro-scale Mode I initiation and propagation [11] places emphasis on understanding the micro-mechanisms occurring under such failure. The toughness of the interlayer has also been identified as a key factor influencing G_{IC}, as opposed to interlaminar thickness, which is thought to be the key factor for increasing G_{IIC} [9], [12].

Mode I specimens were held under load (with the wedge in place) while being scanned, that allowed identification of smaller cracks, which would not be seen had the crack not been held open, and emphasized the crack opening displacement increase moving further away from the crack tip. Fig. 8 also shows the differences between Mode I and Mode II clearly. From qualitative observation, there seems to be more bridging in Mode I (Fig. 8 (ii)), with multiple locations where there is substantial overlap of micro-cracks (Fig. 8 (iii)) that is not apparent in Mode II tests. In both Mode I and Mode II specimens, there is still particle/matrix de-bonding ahead of a continuous (albeit irregular) crack tip. Echelon crack formation is, by its nature, commonly attributed to Mode II loading, due to the local tensile loading on the echelon crack segments. However, in these particle-toughened systems, particle/matrix de-bonding in Mode I appears to coalesce in a manner that is geometrically quite similar to echelons in untoughened systems.

Fig. 9 highlights the microstructural difference in interlaminar thickness over a 0.5mm length ranging from ~20µm to 40µm. The image also shows a straight crack ~45 degrees through a particle-depleted zone that connects a region of particles/resin de-bond to what appears to be a fibre/matrix interface de-bond. In a previous study, this interfacial failure was identified as the dominant propagation mechanism in base (untoughened) laminates under both fatigue and static loading conditions [13]. However, the presence of the particles and subsequent de-bonding and crack coalescence occurring prior to such brittle cracking (supported by Fig 5), the crack is deflected back into the resin rich layer where the prior damage is present. This behaviour may be key, since more energy absorption is expected in the interlaminar region as opposed to the intralaminar region, which

has been reported in the particle toughened T800H/3900-2 material that exhibits a drop in G_{IC} attributed to the transition to the untoughened base/lamina interface [13].

4 Conclusions

Variations in the mechanistic processes and associated geometry of fracture micromechanisms (incipient micro-cracking, deflection, ligament formation) have been assessed in terms of load conditions, revealing variations with corresponding implications for physically representative modelling. Microstructural differences in interlayer thickness (particle size and distribution) clearly influence the fracture micro-mechanisms present. In particular, the local conditions conducive to initial particle-resin separation, the extent of local particle-particle interaction, the geometry of coalescence with the main crack front and the degradation of ligament integrity as it moves further from the crack tip and local crack opening displacements (COD) increase.

Acknowledgements

The authors gratefully acknowledge Cytec Engineered Materials, in particular Dr. Kingsley Ho, for materials supply. The authors acknowledge Sally Irvine and the staff at the TOMCAT/SLS beamline, and Dr. Anna Scott from the μ-VIS X-ray Imaging Centre, Southampton.

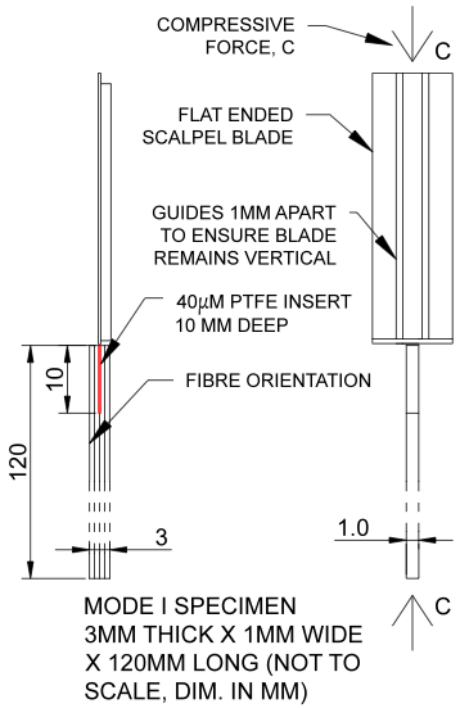

Fig.1A Mode I specimen and wedge arrangement

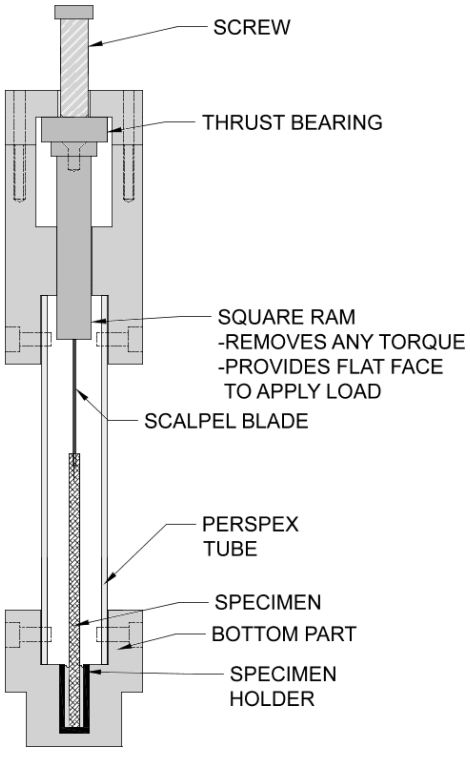

Fig. 1B Compression rig with specimen arrangement as in Fig. 1A

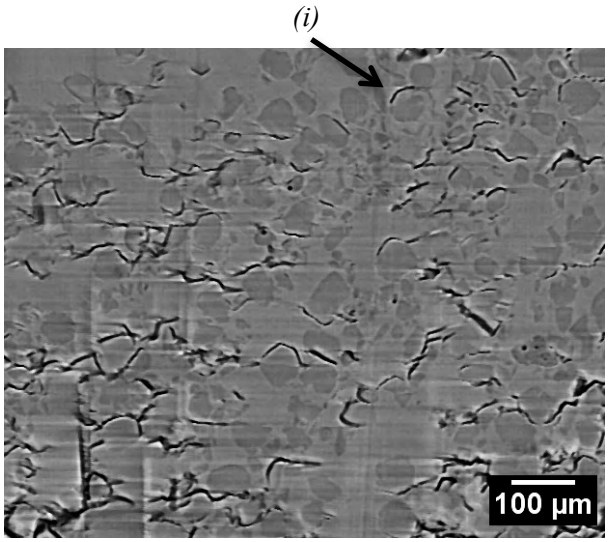

Fig. 2 Plan view of a delamination crack tip in impact, identifying (i) particle-resin de-bonding ahead of the main crack.

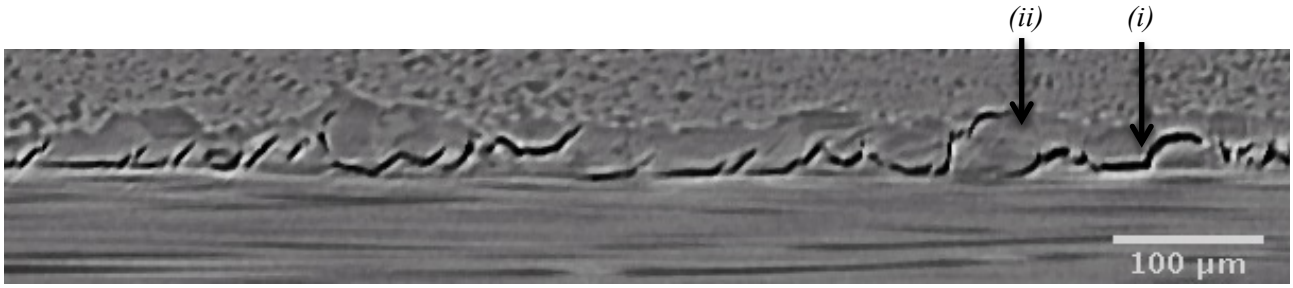

Fig. 3 Side view of an interlaminar crack in a particle-toughened system post impact showing (i) crack deflection and (ii) particle bridging

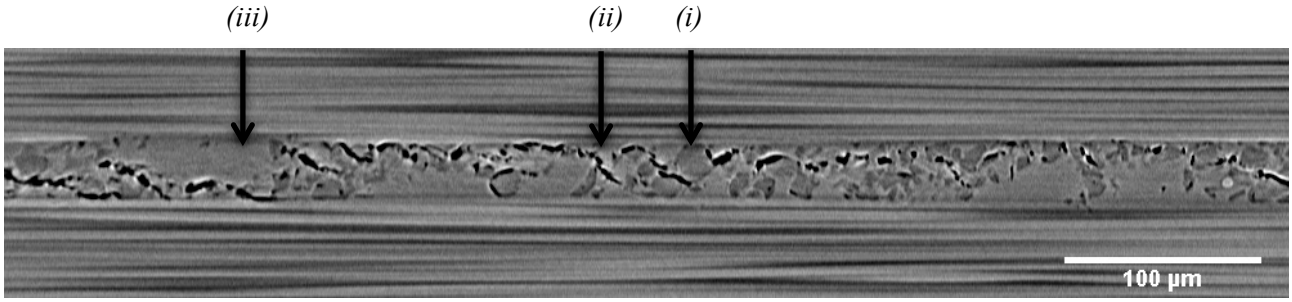

Fig. 4 Side view of a Mode II crack showing (i) particle bridging, (ii) echelon behaviour and (iii) crack path following particle rich zones.

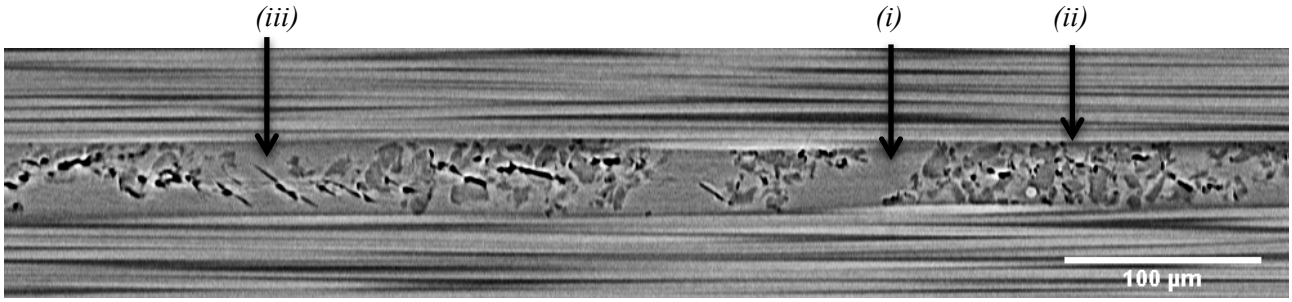

Fig. 5 Side view of a Mode II crack tip showing (i) a particle-depleted region, (ii) particle/matrix de-bonding occurring ahead of a continuous crack, and (iii) echelon behaviour in a particle-depleted zone.

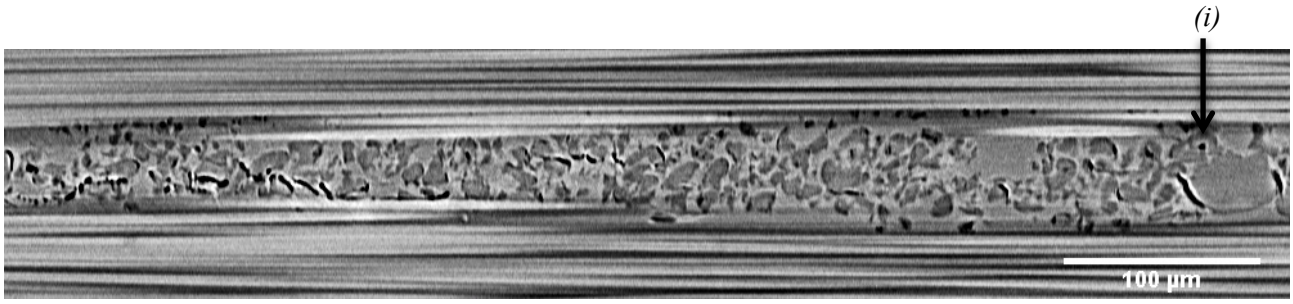

Fig. 6 Side view of a Mode II crack, identifying (i) substantial particle/matrix de-bonding around a large particle ahead of the crack tip

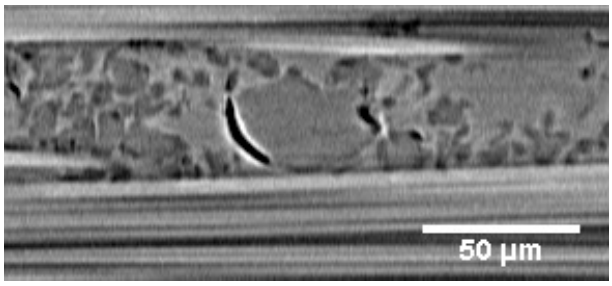

Fig. 7A Shows the particle/matrix de-bonding primarily around the larger particle seen in Fig. 6(i)

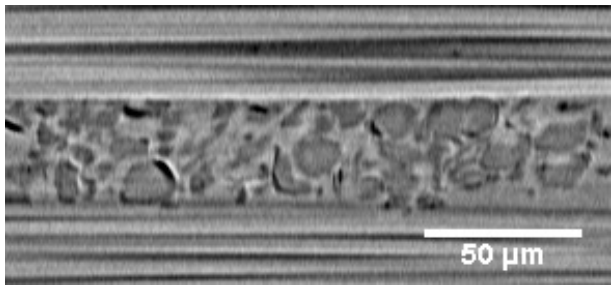

Fig. 7B Shows the same region as in Fig. 7A, but ~30um deeper, where a more uniform distribution of particles gives more uniform de-bonding.

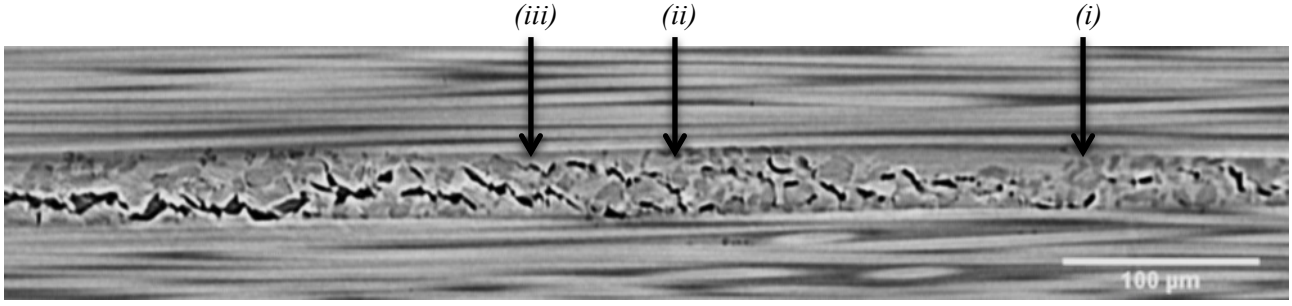

Fig. 8 Near-tip Mode I crack, showing: (i) particle/matrix de-bonding, (ii) bridging, and (iii) overlapping cracks.

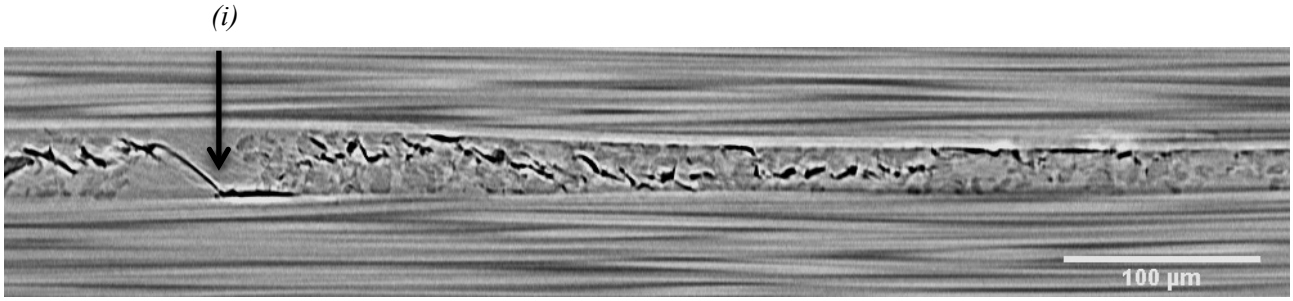

Fig. 9 Crack deviation in a Mode I near-tip region highlighting (i) crack behaviour in a particle-depleted zone

References

[1] S. Sanchez-Saez, E. Barbero, R. Zaera, and C. Navarro, "Compression after impact of thin composite laminates," *Composites Science and Technology*, vol. 65, no. 13, pp. 1911–1919, Oct. 2005.

[2] N. B. A.T. Rhead, R. Butler, "Analysis and compression testing of laminates optimised for damage tolerance," *Applied Composite Materials*, vol. 18, pp. 85–100, 2011.

[3] M. R. Groleau, Y. Shi, A. F. Yee, J. L. Bertram, H. J. Sueb, and P. C. Yang, "Mode II Fracture of Composites Interlayered with Nylon Particles," *Composites Science and Technology*, vol. 56, pp. 1223–1240, 1996.

[4] P. Wright, X. Fu, I. Sinclair, and S. M. Spearing, "Ultra High Resolution Computed Tomography of Damage in Notched Carbon Fiber--Epoxy Composites," *Journal of Composite Materials*, vol. 42, no. 19, pp. 1993–2002, Oct. 2008.

[5] D. J. Bull, I. Sinclair, S. M. Spearing, L. Helfen, U. Kingdom, I. Damage, D. Resistance, S. Radiation, and C. Tomography, "Composite Laminate Impact Damage Assessment by High Resolution 3D X-Ray Tomography and Laminography," pp. 1–6.

[6] P. Cloetens, M. Pateyron-Salomé, J. Y. Buffière, G. Peix, J. Baruchel, F. Peyrin, and M. Schlenker, "Observation of microstructure and damage in materials by phase sensitive radiography and tomography," *Journal of Applied Physics*, vol. 81, no. 9, p. 5878, 1997.

[7] F. Marone and M. Stampanoni, “GRIDREC software,” *J. Synchrotron Rad.*, vol. 19, pp. 1029–1037, 2012.

[8] W. S. Rasband, “ImageJ.” National Institute of Health, http://imagej.nih.gov/ij/, Bethesda, Maryland, USA, 2012.

[9] M. Hojo, T. Ando, M. Tanaka, T. Adachi, S. Ochiai, and Y. Endo, “Modes I and II interlaminar fracture toughness and fatigue delamination of CF/epoxy laminates with self-same epoxy interleaf,” *International Journal of Fatigue*, vol. 28, no. 10, pp. 1154–1165, Oct. 2006.

[10] M. Yasaee, I. P. Bond, R. S. Trask, and E. S. Greenhalgh, “Mode II interfacial toughening through discontinuous interleaves for damage suppression and control,” *Composites Part A: Applied Science and Manufacturing*, vol. 43, no. 1, pp. 121–128, Jan. 2012.

[11] S. Singh and I. K. Partridge, “Mixed-Mode Fracture in an Interleaved Carbon-Fibre/Epoxy Composite,” *Composites Science and Technology*, vol. 55, no. 95, 1996.

[12] H.-M. Hsiao, C.-N. Ni, M.-D. Wu, and C.-W. Lin, “A novel optical technique for observation of global particle distribution in toughened composites,” *Composites Part A: Applied Science and Manufacturing*, vol. 43, no. 9, pp. 1523–1529, Sep. 2012.

[13] M. Hojo, S. Matsuda, M. Tanaka, S. Ochiai, and A. Murakami, “Mode I delamination fatigue properties of interlayer-toughened CF/epoxy laminates,” *Composites Science and Technology*, vol. 66, no. 5, pp. 665–675, May 2006.